Front. Struct. Civ. Eng. 2024, 18(12): 1829–1844
https://doi.org/10.1007/s11709-024-1116-9

RESEARCH ARTICLE

Performance of eco-friendly lightweight concrete in-filled Fiber Reinforced Polymer composite columns under axial compression——An experimental, numerical, and theoretical approach

Varunkumar VEERAPANDIAN, Gajalakshmi PANDULU*, Revathy JAYASEELAN

Department of Civil Engineering, B. S. Abdur Rahman Crescent Institute of Science & Technology, Chennai 600048, India
**Corresponding author. E-mail: gajalakshmi@crescent.education*

ABSTRACT In this study, innovative Lightweight Self-compacting Geopolymer concrete made of industrial and agricultural wastes is developed and used as the in-fill material in Fiber Reinforced Polymer (FRP) composite columns. The axial compressive performance of the columns is investigated with critical parameter variations such as the effect of the Diameter to thickness (D/t) ratio and fiber orientation of the FRP tube. Two types of D/t ratios, i.e., 30 and 50, and three fiber orientations ±0°, ±30°, and ±45° were used for the key parameter variations. An increased D/t ratio from 30 to 50 reduces the performance in terms of load despite increasing the deformation. The columns containing the fiber orientation of ±0° exhibit greater performance compared to other types of fiber orientation (±30° and ±45°). The experimental results and failure patterns were compared and validated against the numerical and theoretical studies. A Finite Element model is developed and validated with the experimental results with errors ranging from 0.84% to 4.57%. The experimental results were validated against various existing theoretical prediction models with a percentage error of 7% to 14% An improved theoretical model is proposed for predicting the axial load of concrete-filled FRP composite columns.

KEYWORDS lightweight concrete, geopolymer concrete, axial compressive loading, FRP composite columns, fibre orientations, diameter to thickness ratio

1 Introduction

Researchers were focusing on developing substitute binder materials for Ordinary Portland Cement (OPC), primarily because cement manufacture needs a considerable amount of energy and releases a substantial amount of CO_2 into the environment [1]. For the building industry to be sustainable, alternative structural materials to this OPC might be employed [2].

Geopolymer Concrete (GPC) technology has recently gained attention due to its significantly lower CO_2 emissions than OPC with better mechanical characteristics and durability [3,4]. Based on the findings of existing research, GPC offers greater tensile and bending properties [5,6]. The concept of "geopolymer" was first used by Davidovits to characterize the materials produced by the polymerization of silicon and aluminum-rich fly ash and alkaline liquid [7]. To minimize environmental contamination, GPC makes use of industrial and agricultural waste instead of disposing of it [8]. Numerous investigations on GPC utilized fly ash as their major constituent, which needs high temperatures for curing to attain the desired concrete strength [9,10]. Extended curing may break the granular structure of fly ash-based geopolymers. Flyash has comparatively poor reactivity with other components because it is devoid of calcium, which extends the setting time of concrete. To counteract this, calcium-rich materials such as Ground Granulated Blast Furnace Slag (GGBS) can be employed, which has been shown to improve the polymerization reaction. Due

Article history: Received May 10, 2023; Accepted Mar 8, 2024

to their pozzolanic characteristics, the industrial and agricultural wastes GGBS and rice husk ash (RHA) are employed as alternative binders for OPC [11–14]. Previous studies have shown that the GGBS avoids temperature curing without decreasing its compressive strength [15]. Compared to Flyash-based GPC, GGBS-based GPC offers a significantly enhanced compressive strength at ambient temperature [16]. Recent research revealed that partial substitution of RHA with GGBS enhances the mechanical and microstructural properties [17].

Advancement in Self-Compacting Concrete is necessary for application in structures with congested reinforcement as it consolidates under its weight [18]. However, studies on Self-Compacting Geopolymer Concrete (SCGC) are still in their initial stages. It is crucial to decrease the self-weight of the structural components to decrease the dead load of the structure. Lightweight Self-Compacting Geopolymer Concrete (LWSCGC) is a sustainable strategy, although very few investigations have been done on its properties. It can be employed in constructions in earthquake-prone zones due to its reduced weight, better compaction, improved bond strength with reinforcement, greater strength-to-weight ratio, low cost of transportation, and smaller foundation size. Lightweight Expanded Clay Aggregate (LECA) has now been widely employed as an alternative to conventional coarse aggregate (CA) due to its lesser weight and better endurance [19,20]. It demonstrates that the workability of concrete specimens incorporating LECA in the size range of 4.75 to 20 mm is greater than their corresponding specimens made with conventional CA [21]. Based on the temperature-time curve ISO 834, concrete made with LECA aggregate does not deteriorate when subjected to high temperatures and it has incredible potential for environmental sustainability and fire resistance as a green construction material [22,23].

Researchers have been exploring using Fiber Reinforced Polymer (FRP) composites for concrete confinement by upgrading existing columns or developing new ones like Concrete-Filled Fiber Tube (CFFT) columns. GPC in-filled FRP composite columns have been challenging due to its brittle nature, but using FRP tubes has been found to mitigate this issue. Studies have shown that OPC and GPC in-filled Glass–Fiber Reinforced Polymer (GFRP) tubes have a significantly greater ultimate strain than CFRP and BFRP tubes without internal reinforcement. Additionally, sisal-reinforced FRP-confined concrete cylinders gain strength under temperature variations. In contrast, Full Lightweight Aggregate concrete in-filled Direct Strength Transfer Connections (DSTCs) increase in strength due to being confined between FRP and steel. Researchers have studied the performance of SCGC in-filled HDPE tubes under flexural loading and found that the CFRP-concrete composite action enhances the performance of columns subjected to thermal and structural loading [24–38].

Researchers have conducted extensive investigations into the viability of using FRP composites for concrete confinement. The effectiveness of the FRP tube is mainly dependent on the material characteristics, volume fractions, types, orientations of the fibers, and tube thickness. Numerous studies have examined the impacts of these factors, revealing that an increase in the volume fraction of fibers significantly enhances tensile strength. Furthermore, research has demonstrated that the type of fiber utilized significantly impacts the performance of high-strength concrete in-filled FRP tubular columns. Altering the position and width of partial Carbon-FRP (CFRP) wraps has improved the axial stress-strain behavior of concrete specimens. However, there is no significant difference in performance between various configurations of discontinuous CFRP laminate strips [39–42].

The behavior of CFFT columns is significantly impacted by tube thickness and fiber orientations. However, a lack of comprehensive research in this area has necessitated further investigation. An exploratory study examined the effect of FRP thickness on a set of composite columns fabricated with glass fibers, each tube oriented at a 15° angle. The research team studied the uni-axial compressive behavior of concrete columns jacketed with FRP composites at angles of 0°, 45°, and 90° while also considering the effects of different fiber orientations, fiber types, and FRP thickness. The experimental outcomes were validated using theoretical models to examine the efficiency of CFFT columns with fiber angle orientations of 55° and 77°. A subsequent study investigated the Aramid-type DSTCs of FRP tube thickness of 4 to 6 layers under axial compression, revealing a significant increase in load performance with increasing FRP layer thickness. Previous research has indicated that various types of fiber angle orientations and FRP tube thickness can influence the behavior of these composite columns. However, further research is necessary to gain an in-depth understanding of the effects of these parameters [43–46].

Implementing FRP-confined composite columns has been a topic of extensive experimental research. However, numerical and theoretical studies have been relatively sparse. A recent study utilized numerical and theoretical methods to predict the structural performance of FRP-confined steel tubular concrete columns [47]. The analytical equations presented by the American Concrete Institute (ACI) and the Canadian Standards Association (CSA) for Building Code [48,49] have been widely adopted in the industry to estimate the load capacities of confined reinforced concrete columns. Moreover, a recent experimental study examined the mechanical properties of CFRP-confined rectangular concrete-filled steel tube

stub columns subjected to axial compression loading. It proposed a prediction method for determining the bearing capacity [50]. The study found that the stiffness and strength of the confined concrete can be significantly enhanced by using CFRP, which opens up exciting possibilities for future construction projects. Despite these efforts, accurately estimating the load capacities of concrete in-filled FRP composite columns remains challenging due to the complexity of the interaction between different materials. Furthermore, the number of numerical and analytical studies on this type of lightweight concrete in-filled FRP composite columns is relatively limited, indicating a significant knowledge gap that requires further investigation.

This research aims to develop a new type of sustainable material, LWSCGC, created using industrial and agricultural waste. The material is designed to meet specific standards, including being lightweight, possessing self-compacting properties, and being a geopolymer material. The primary objective of the study is to investigate the behavior of LWSCGC filled-in GFRP tubular columns reinforced with steel under axial compressive loading. The study examines the efficiency of LWSCGC-GFRP composite columns and the effects of various fiber orientations and diameter-to-thickness ratios on the material's performance. The research involves a detailed experimental program that includes testing of LWSCGC-GFRP composite columns under different loading conditions. The study also consists of a numerical analysis using Finite Element software to develop a numerical model that comprehensively analyses the behavior of these composite columns.

The load−deformation behavior, strain characteristics, failure pattern, and other impacts of LWSCGC are analyzed in detail. The research aims to contribute to understanding the sustainability and potential applications of this type of lightweight composite material in the construction industry. The experimental test results are compared with existing theoretical models to validate the proposed model. The study presents an improved theoretical model that can determine the load capacity of the concrete-filled composite columns. This model is validated with the experimental data and can predict the behavior of these composite columns in various design scenarios. The research findings offer significant insights into the behavior of LWSCGC and its potential applications in the construction industry. This study can lead to the development of lightweight composite materials that can be used in various structural applications, such as bridges, buildings, and other infrastructure. The results of this study can also contribute to the reduction of waste materials and the development of sustainable construction practices. In summary, this research contributes significantly to developing sustainable materials in the construction industry. Its research findings provide essential insights into the behavior of LWSCGC and its potential applications in developing sustainable and cost-effective structures.

2 Experimental study

2.1 Materials

2.1.1 Lightweight self-compacting geopolymer concrete

In this investigation, the LWSCGC is developed and utilized. The main binder for making the concrete mixture is comprised of GGBS and RHA. The fine aggregate (FA) utilized in this study is manufactured sand (M-sand). Regular CA (size 10 to 12 mm) and LECA (size 10 to 15 mm) were used. To initiate the polymerization, an alkaline activator is made by combining sodium hydroxide (NaOH) and sodium silicate (Na_2SiO_3) solutions. Using pellets of NaOH, a NaOH solution with an 8 molar concentration was prepared. The mix proportion for NaOH to Na_2SiO_3 was 1:2.5. To obtain the necessary workability, the polycarboxylic ether-based superplasticizer (SP) is employed.

Fresh concrete was produced by first blending the binder components, and FA, in a pan mixer under dry circumstances for 3–4 min. 75% of water can be added to the dry mixture to hydrate it. In addition, 75% of an alkaline activator is added to the mixture. The SP was incorporated into the mixture along with the remaining 25% of the water. The SP and water activate the alkaline solution, causing polymerization to take place. The next step is to include LECA and CA into the mixture. The remaining 25% of the alkaline activator is incorporated into the mix, and wet mixing should last 3–4 min. The mix design for this LWSCGC is presented in Table 1. The density of this concrete (LWSCGC) is 1838 kg/m^3 and hence it can be utilized in the structural members as per the codal provisions.

To examine the characteristics of developed fresh concrete (LWSCGC), several tests were conducted under the recommendations of the European Federation of National Associations Representing for Concrete (EFNARC) [51].

Table 1 Mix design for LWSCGC

Materials	Quantity (kg/m^3)
GGBS	381
RHA	4
FA	1015
CA (Conventional)	406
LECA	120
Alkaline Activator	341
Extra water	98
SP	28

The slump flow was calculated by considering the diameter of the flow on various sides. The measured slump flow of the LWSCGC is shown in Fig. 1. The T-50 slump flow indicates the number of seconds required for the slump flow to cross a 50 cm diameter. For V-Funnel, fresh concrete is filled in the V-portion and made to pass through the bottom door. The number of seconds required for the concrete to flow through the section entirely was calculated. The flown concrete is then refilled into the section, and after 5 min the door was opened and the time is measured for the V-Funnel $T_{5\ min}$ test. For the L-Box experiment, the concrete is filled in the vertical section and allowed to flow through the lateral sections and the ratio of heights in both sections was calculated. Table 2 illustrates the permissible values for the various tests according to EFNARC guidelines [51] along with the test results.

Fig. 1 Slump flow of the LWSCGC.

Table 2 Fresh properties test results of LWSCGC

Tests performed	Unit	Permissible limits	Test results
Slump flow	mm	650–800	682
$T_{50\ cm}$ slump flow		2–5	5
V-Funnel	s	6–12	7
V-Funnel $T_{5\ min}$		6–12 (±3)	8
L-Box		0.8–1	0.92

The hardened properties of LWSCGC were tested to evaluate its mechanical characteristics, and the 28-d test results for the compressive and flexural strengths were 18.3 and 3.8 MPa, respectively. Therefore, the developed concrete (LWSCGC) mix satisfied the required fresh and hardened properties as per the EFNARC guidelines and Indian Standards (IS) codal provisions. Hence, This developed concrete (LWSCGC) can be filled in the GFRP tubes for employing it as an efficient structural member.

2.1.2 Glass–Fiber Reinforced Polymer tubes

The FRP tubes were manufactured by filament winding and GFRP type tubes were employed in this study as presented in Figs. 2(a) and 2(b). Filament winding is widely used to manufacture pipes for industrial purposes, as the technique involves wrapping glass roving filaments tightly around a rotating mandrel infused with resin. After the resin is cured, the mandrel is removed, and a hollow product is left behind. In the case of liquid or gas tanks, the mandrel serves as a permanent liner. Filament winding is a dependable method for producing lightweight, long-lasting, and highly corrosion-resistant products. It also allows the creation of customized shapes and sizes with great precision and control. This makes it possible to manufacture products with intricate designs and geometries.

As illustrated in Fig. 3, different fiber orientations (±0°, ±30°, and ±45°) were used with the E-glass fiber and epoxy resin along the longitudinal direction. These tubes have the same internal diameter of 150 mm with different thicknesses (3 and 5 mm). According to ASTM D3039M-08 [52] and ASTM D2290-08 [53], the longitudinal and hoop tensile tests were performed for the GFRP coupons and ring specimens. The test setup and results were presented in Fig. 4 and Table 3. The GFRP coupons and ring specimens underwent longitudinal and hoop tensile tests following the established standards of ASTM D3039M-08 [52] and ASTM D2290-08 [53]. The longitudinal tensile tests were carried out by applying a uniaxial load along the length of the GFRP coupons. In contrast, the hoop tensile tests were performed using a circumferential load around the ring specimens. A detailed representation of the test setup and the results of

(a) (b)

Fig. 2 GFRP tubes: (a) front view; (b) top view.

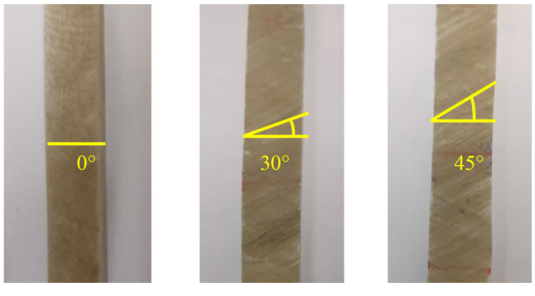

Fig. 3 GFRP samples with different fiber orientations.

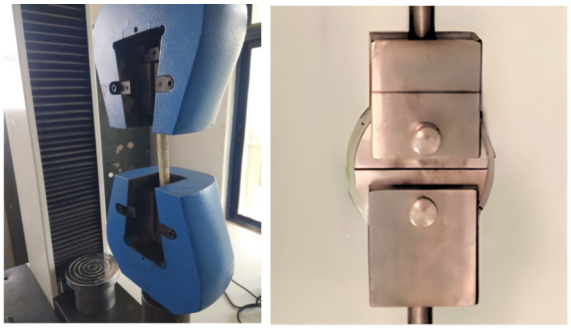

(a) (b)

Fig. 4 Test setup for longitudinal and hoop tensile tests: (a) longitudinal direction; (b) hoop direction.

the experiments have been presented in Fig. 4 and Table 3, respectively. The data obtained from these experiments can significantly contribute to developing GFRP structures in various engineering applications. In conclusion, the results of these experiments highlight the strength and stiffness of GFRP coupons and ring specimens and provide valuable insights for their application in real-time scenarios.

Upon close examination, it was determined that GFRP coupons and ring specimens, with a thickness of 5 mm and 0° fiber orientation, exhibited superior tensile properties in longitudinal and hoop directions compared to the remaining specimens. These findings suggest that the thickness and fiber orientation of GFRP specimens play a crucial role in determining their tensile properties and should, therefore, be considered during the design and production of such components. It is essential to note that the results of this study have significant implications for the development and optimization of GFRP materials for a wide range of industrial and academic applications.

2.1.3 Steel reinforcement

The Fe-415 type of steel bars was used for steel reinforcement. Six steel bars with 12 mm diameter are used for the longitudinal reinforcement and steel bars with 8 mm diameter are used for the lateral reinforcement with 120 mm c/c spacing as presented in Figs. 5 (a) and 5(b). The covers were given at 40 and 20 mm in the longitudinal and lateral directions correspondingly. The tensile coupon tests were performed for the steel reinforcement bars as per ASTM A370-20 [54] standards for determining the tensile properties. The reinforcement steel bars have a tensile strength of 426.5 N/mm^2 and a Poisson's value of 0.3, respectively.

2.2 Test specimens

Six LWSCGC-GFRP composite columns, each filled with LWSCGC, were cast and examined subjected to axial compression. Throughout the process, utmost care was taken to ensure that the strength of the in-filled concrete, reinforcement details, and column height remained consistent. However, these two factors were systematically varied to examine the impact of D/t ratio and fiber orientation. This meticulous approach allowed for a more detailed and comprehensive analysis of the effects of the D/t ratio and fiber orientation on the overall structure. Three fiber orientations (±0°, ±30°, and ±45°), as well as two D/t ratios (30 and 50) of FRP tubes, were employed in this study. The height of each specimen is 1000 mm and steel reinforcement is provided for every specimen. The inner diameter of each specimen is 150 mm, whereas the outer diameters are 156 and 160 mm respectively. The typical sectional view and in situ LWSCGC in-filled GFRP composite columns were shown in Figs. 6(a) and 6(b).

The specimens were assigned the letters L for the type of concrete used (LWSCGC), and G for the FRP tube (GFRP tube). The letters DT and F indicate the D/t ratio and fiber orientation and number before the letters DT and F represent the details of the D/t ratio and fiber orientations, respectively. For example, the specimen LG-50DT0F represents that LWSCGC in-filled GFRP tubular column having the D/t ratio of 50 and ±0° fiber orientation. The description of the test specimens were illustrated in Table 4.

2.3 Formwork, and casting

The inner surface of the GFRP tubes was nail scratched

Table 3 Tensile properties of GFRP tubes

Fibre type	Thicknes (mm)	Fibre winding angle (°)	Tensile modulus (MPa)		Tensile strength (MPa)		Elongation (%)
			Longitudinal	Hoop	Longitudinal	Hoop	
GFRP	3	±0	3745.31	8763.3	38.62	91.14	1.66
		±30	3469.14	7944.01	34.28	79.19	1.57
		±45	3316.69	7427.84	33.91	76.64	1.36
	5	±0	4537.74	11298.97	46.89	117.69	5.55
		±30	4224.78	10308.46	43.11	106.05	4.79
		±45	4205.79	10051.84	42.10	101.46	3.90

for superior bonding between the in-filled concrete and GFRP tubes. A wooden setup is prepared for placing the GFRP tube within it and to ensure better safety while and after casting. The reinforcement steel is provided within the GFRP tube and corresponding longitudinal and lateral covers were given. The lower portion is sealed with a foil sheet to limit the concrete within it and placed in the wooden setup in which the sand is filled around it to support its stability. The developed concrete (LWSCGC) is cast inside the GFRP tube and left for a better setting. After 3 d, the columns were taken out and sealed foil sheets were removed and maintained at ambient curing over 28 d. The formwork, casting, and curing of these

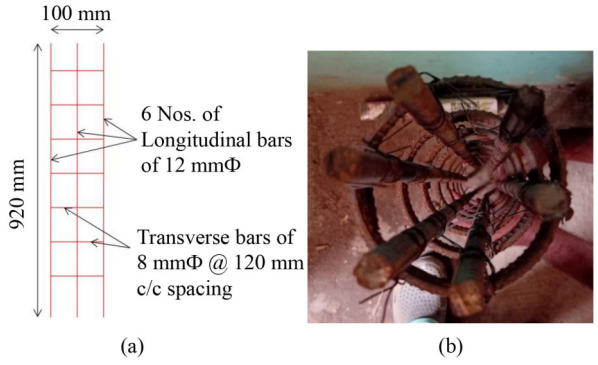

Fig. 5 Steel reinforcement details: (a) typical sectional details of steel reinforcement; (b) *in situ* steel reinforcement.

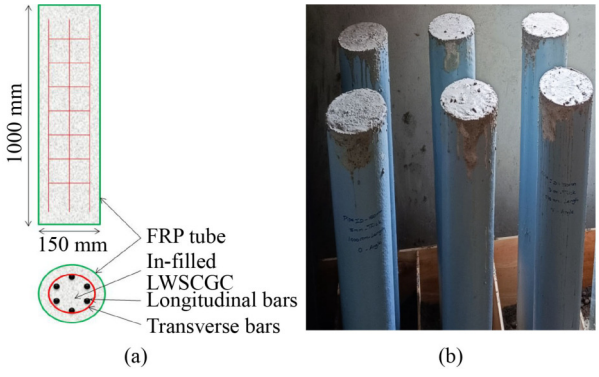

Fig. 6 LWSCGC in-filled GFRP tubular columns: (a) typical sectional view of LWSCGC-GFRP composite columns; (b) *in situ* LWSCGC-GFRP composite columns.

Table 4 Specifications of columns

Column label	Concrete type	Type of FRP tube	Column height (mm)	*D*/*t* ratio	Fiber orientation (°)
LG-50DT0F	LWSCGC	GFRP	1000	50	±0
LG-50DT30F					±30
LG-50DT45F					±45
LG-30DT0F				30	±0
LG-30DT30F					±30
LG-30DT45F					±45

LWSCGC-GFRP composite columns were presented in Figs. 7(a)–7(d).

Fig. 7 Formwork and casting of LWSCGC-GFRP composite columns: (a) GFRP tube sealed at the bottom; (b) GFRP tube with reinforcement; (c) casting of concrete; (d) formwork for casting.

2.4 Instrumentation, test setup, and loading

A base setup has been prepared with a holder for placing the column without any difficulties. The column is placed and two linear variable displacement transducers (LVDTs) are connected to the upper plate to record the axial deformation. Eight 120 Ω strain gauges were positioned at the center of the column with each two on the four opposite sides to calculate the axial and hoop strain data as illustrated in Fig. 8(b). A 2000 kN hydraulic jack along with the loading frame is employed for the application of loading at a rate of 2 kN/s [55]. The loading was monitored with the help of the load cell positioned in between the hydraulic jack and the column. The data acquisition system connected to the computer was employed to synchronize the load cell, LVDTs, and strain gauges. The experimental test setup for axial loading of these LWSCGC-GFRP composite columns is presented in Fig. 8(a).

3 Numerical modeling

These LWSCGC-GFRP composite columns were modeled using FE software for the validation of the experimental results.

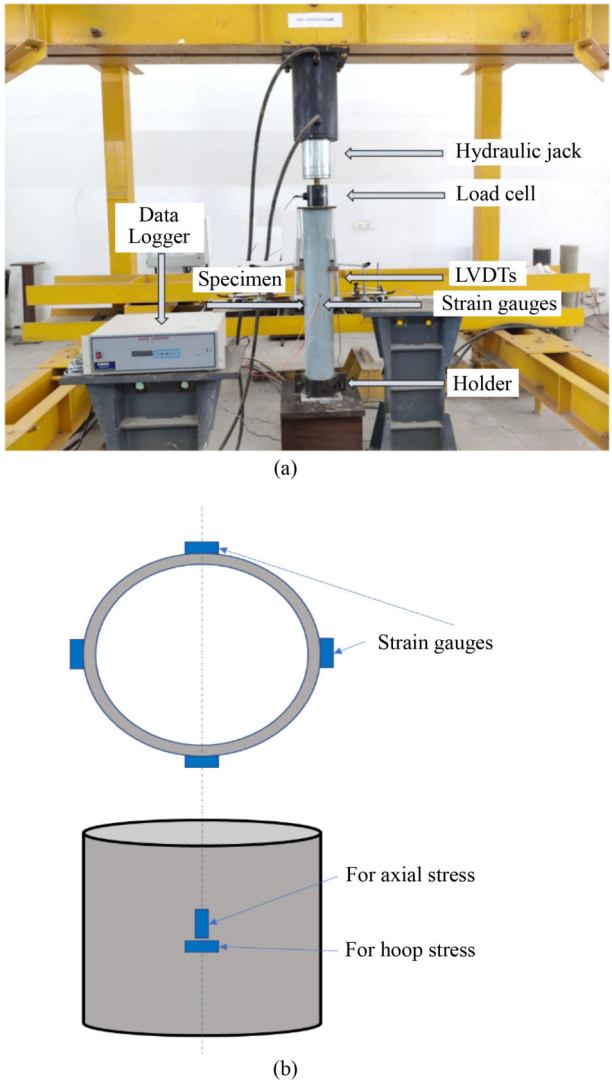

Fig. 8 Test setup and Instrumentation details: (a) test setup for axial compressive loading; (b) positioning of strain gauges.

3.1 Material modeling

Three components were modeled for modeling LWSCGC-GFRP composite columns namely the in-filled concrete, GFRP confinement tube, and steel bars.

The concrete (LWSCGC) is characterized by a 3-dimensional 8-nodded solid brick element accompanied by reduced integration. The properties of the in-filled concrete LWSCGC are assigned using the Concrete Damage Plasticity model. The solid homogeneous element has been adopted for the sectional characteristics.

A 3-dimensional 4-nodded doubly curved shell element was adopted for modeling the GFRP tube. The elastic property is provided with the classical laminate theory and the material type 'Lamina' is applied. The Hashin damage model was employed for damage property for the characterization of damage to the GFRP tubes. The homogeneous shell element along with composite lay-up was assigned for the sectional property. A 3-dimensional truss element has been employed for modeling the steel reinforcement with reduced integration and the elastic property has been assigned. The developed finite element model of different components such as confined concrete, GFRP tube, steel reinforcement and skeletal view of the composite column was presented in Fig. 9.

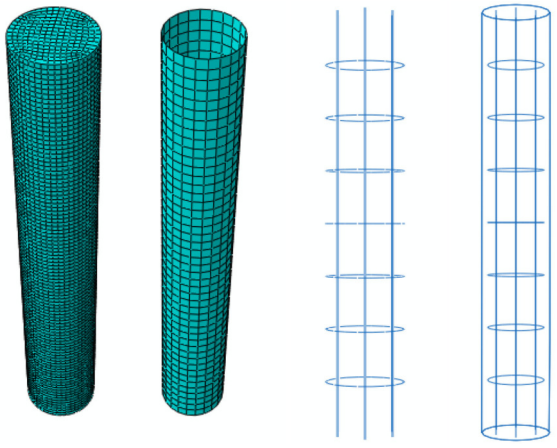

Fig. 9 FE modeling of different components such as confined concrete, GFRP tube, Steel reinforcement and the skeletal view of the composite columns.

3.2 Interactions, boundary conditions, and loading

The interaction between these components was applied to avoid any bonding defects. The hard interface is assigned between the in-filled concrete (LWSCGC) and the GFRP tube to counteract any penetration. The contact surface of concrete and GFRP tube were categorized as the master and slave surfaces. In the tangential direction, the frictional interaction is assigned between the in-filled concrete and the outer GFRP tube, and the frictional co-efficient is kept at 0.5 [56,57]. The hard contact surface is applied in between the in-filled concrete and steel bars where the in-filled concrete and steel bars are the master and slave surfaces respectively.

The reference points were created on the upper and lower ends and provided with the constraints. The column is entirely restricted at the lower end and restrained against the longitudinal direction at the upper end. The displacement-controlled load is assigned on the entire top surface as axial compression.

4 Test observations and discussions

4.1 Experimental study

4.1.1 Failure patterns

The failure modes observed in all LWSCGC-GFRP

composite columns, regardless of the D/t ratio and fiber orientations, were quite common and consistent. During the initial stages of loading, no visible failure modes were detected in any of the components, including the reinforcement bars, concrete, and the outer GFRP tube. However, as the load was gradually increased, the reinforcement bars and concrete began to fail, leading to the development of small micro-cracks on the outer GFRP tube. Compressive concrete failure was observed as the loading continued, accompanied by a loud sound, and rupture developed in the GFRP tube. It was observed that the compressive failure of concrete occurred diagonally, and the loss progressed gradually from the bottom to the top of the column. The failure of the reinforcement bars was also observed to happen gradually, with the bars exhibiting significant deformation before they eventually failed.

Upon failure, the load decreased, and the column could no longer bear any additional load. The ultimate failure loads of these LWSCGC-GFRP composite columns ranged from 554.18 to 702.67 kN, and it is worth noting that the failure loads were found to be independent of the D/t ratio and fiber orientations. Figure 10(a) provides a visual representation of these LWSCGC-GFRP composite columns after failure, highlighting the extensive damage caused by the failure of the reinforcement bars and concrete. The significant damages suffered by the columns due to the rupture of the GFRP tube and the compressive failure of concrete emphasize the importance of considering the loading levels and characteristics of LWSCGC-GFRP composite columns carefully. It is important to note that the compressive strength of concrete and the tensile strength of the reinforcement bars are crucial factors in the design of these columns. Therefore, a critical evaluation of these factors is necessary to ensure that the columns are structurally safe

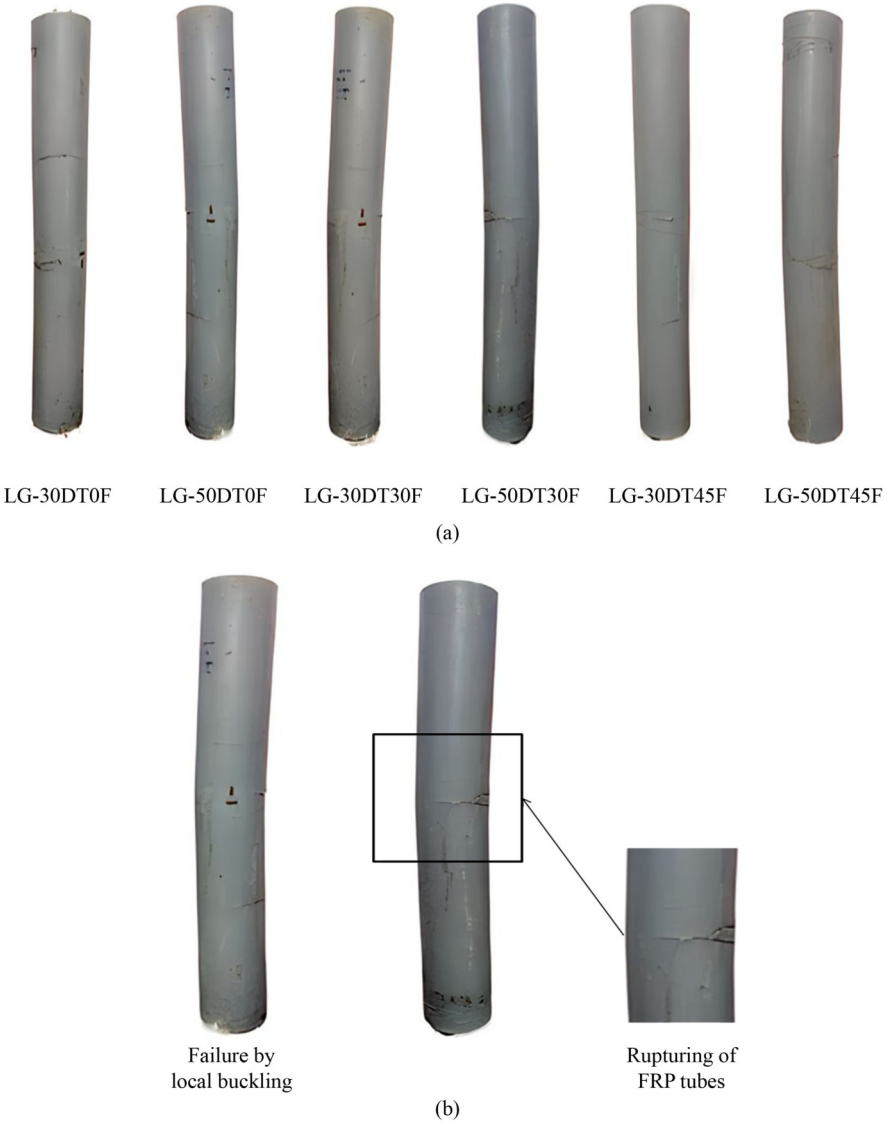

Fig. 10 (a) LWSCGC-GFRP columns after failure; (b) general failure modes of the columns.

under loading conditions.

The confinement and load-carrying capacity of a structural column is influenced by several factors, including its D/t ratio and fiber orientation. The D/t ratio is critical in determining its ability to withstand loads. Columns with lower D/t ratios generally provide superior confinement due to the greater column thickness, resulting in a higher confinement ratio and greater strength. Additionally, columns with a 0° fiber orientation exhibit outstanding performance in load-carrying applications, as the perpendicular bi-directional fiber alignment of the GFRP tube provides better confinement and support, enabling the column to withstand greater loads. The optimal selection of D/t ratio and fiber orientation is pivotal in ensuring the optimal performance of GFRP columns in structural applications. By carefully considering these factors, engineers can design GFRP columns that meet the required strength and load-carrying capacity for a given application. Thus, understanding the relationship between the D/t ratio, fiber orientation, and the load capacity of a column is essential in designing GFRP columns for structural applications.

The failure modes of these LWSCGC in-filled GFRP composite columns were first the compressive failure of concrete along with rupturing of the GFRP tubes. Some other modes were also observed in these LWSCGC-GFRP columns which include local buckling and interfacial bonding failure of the GFRP tube and concrete (LWSCGC) as well as the concrete (LWSCGC) and the steel reinforcement bars. These buckling failures can be seen almost in every column and bonding failure is observed in some of the columns. Upon conducting an in-depth analysis, it has been revealed that the rupturing of the GFRP tube typically occurs in the mid-height region, which spans between 400 and 650 mm for almost all columns. Moreover, it has been observed that the buckling displacement of columns is directly proportional to their D/t ratio. This is due to the fact that columns with a higher D/t ratio have thinner GFRP tubes, which lead to a reduced confinement ratio. As a result, the columns exhibit a higher buckling displacement due to the reduced strength of the GFRP tube in these regions. Therefore, the buckling displacement of columns can be controlled by adjusting their D/t ratio and using a GFRP tube with an appropriate thickness to maintain a higher confinement ratio. The rupturing occurs in the center portion of the columns due to the excessive stress generated from the compressive failure of the concrete. No rupture or buckling failures were seen visually until the load reaches 350 to 400 kN. The rupturing of the GFRP tube and the local buckling were noticed when the load increases gradually beyond this 350 to 400 kN. This change was mainly due to the load transformation from the in-filled concrete to the outer GFRP tube from which the following failure modes were observed. The physical changes in the composite columns were reflected in the load and deformation behavior where the gradual increase in the deformation could be noted beyond this level of 350 to 400 kN. The general failure modes of these LWSCGC-GFRP composite columns were presented in Fig. 10(b).

Every LWSCGC-GFRP composite column exhibits a similar failure pattern as illustrated in Fig. 11. The failure modes seen in the FE modeling were primarily GFRP tube rupturing, characterized by local buckling of the columns. From Fig. 11, it is evident that the high-stress distribution is observed in the center of the columns. Comparatively, the initial rupturing is observed in the mid-portion in the conducted experiments, and the local buckling and rupturing were evidenced in both experimental and FE modeling. Hence, no changes in the interfacial bonding between the GFRP tube and in-filled concrete as well as the in-filled concrete and steel reinforcement were observed in the LWSCGC-GFRP columns even the co-efficient of friction changes. The interfacial bonding failure between the GFRP tube and concrete as well as the concrete and reinforcement bars has been observed only in the experiments.

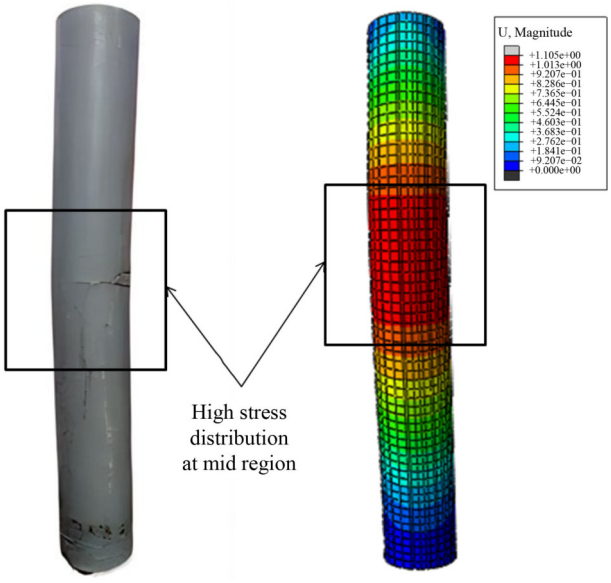

Fig. 11 Comparison of experimental and FE analysis failure modes.

4.1.2 General load-deformation behavior

The LWSCGC-GFRP composite columns almost exhibit a similar load-deformation pattern which is comprised of two primary sections. The first section indicates the gradual increase in load with the corresponding deformation. When it reaches the yield point, the column undergoes yielding and further the load increases with an increase in the deformation. From the curve, it can be

inferred that the entire column withstands the load up to the yield point. At this point, the in-filled concrete (LWSCGC) and the reinforcement steel fail and transform the load to the outer GFRP tube. The yielding stage occurs in the load range of 350 to 400 kN where the LWSCGC-GFRP composite columns containing a lesser *D*/*t* ratio undergo yielding at 400 kN and a greater *D*/*t* ratio undergoes yielding at the load range of 350 kN. From this range, the micro-cracks start developing in the GFRP tube and the process continues until the complete failure load of the composite columns. The deformation of these columns was comparatively less in the first segment than in the second segment. This is mainly due to the ultimate load transformation to the GFRP tubes as the tube ruptures and fails at the end. The typical Load-deformation behavior of these LWSCGC-GFRP composite columns is presented in Fig. 12.

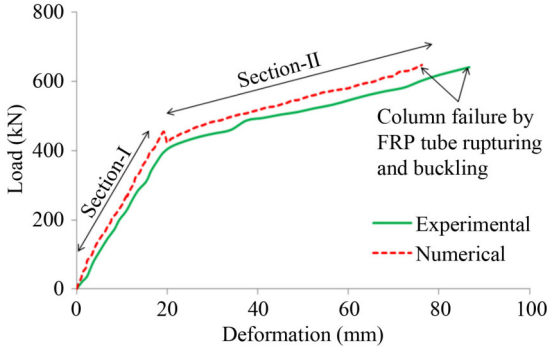

Fig. 12 Typical Load-deformation behavior of LWSCGC composite columns.

In the FE analysis, the Load-deformation curve comprises a linear part and a load drop is observed at the end of the linear part. The drop in load is primarily influenced by the transfer of load from the in-filled concrete to the GFRP tube. The load increases linearly with an increase in the deformation compared to the initial linear curve and reaches the ultimate load. Comparatively, there is no load drop in the experimental curve and the second linear curve with increased deformation is observed in experimental and FE results. The maximum load obtained for the LWSCGC-GFRP composite columns (LG-30DT0F, LG-30DT30F, LG-30DT45F, LG-50DT0F, LG-50DT30F, and LG-50DT45F) in the FE results is 2.19%, 0.95%, 2.10%, 4.57%, 2.80%, and 0.84% greater than the experimental results as presented in Table 5.

4.1.3 Parametric analysis

The influence of two critical parameters, the *D*/*t* ratio, and the fiber orientations was considered upon the Load-deformation behavior of these LWSCGC-GFRP composite columns.

4.1.3.1 The influence of the *D*/*t* ratio

1) Load–deformation behavior

The *D*/*t* ratio has a substantial influence on the overall performance of these LWSCGC-GFRP composite columns and two types of *D*/*t* ratios, i.e., 30 and 50 were employed in this investigation. The performance of the column containing a lesser *D*/*t* ratio is greater than that of a greater *D*/*t* ratio. Increasing the *D*/*t* ratio can yield a significant improvement in the ductility of a structural member. This phenomenon may be attributed to the fact that CFFT columns exhibit enhanced flexibility and reduced rigidity with decreased tube thickness, even though their strength may be comparatively lower than that of other columns. This improved flexibility enables the columns to undergo more significant deformation while maintaining their structural integrity, ultimately leading to superior ductility and structural performance. It is worth noting that these findings can have profound implications for the design of structural systems, especially in the context of seismic-resistant structures where ductility is of paramount importance [58] The efficiency of the columns enhances when the *D*/*t* ratio is lowered from 50 to 30.

Comparing the *D*/*t* Ratio in terms of load-deformation behavior for different fiber orientations in Figs. 13(a)–13(c). From the experimental study, it can be inferred that the performance of columns with a greater *D*/*t* ratio is lesser than the columns with a lesser *D*/*t* ratio. The axial performance of the columns containing the lesser *D*/*t*

Table 5 Comparison of Load and deformation results (Experimental vs FE model)

Column	Load			Deformation		
	Experimental	FE model	Error (%)	Experimental	FE model	Error (%)
LG-50DT0F	594.91	607.39	2.10	95.99	89.36	6.90
LG-50DT30F	557.00	572.61	2.80	96.68	86.21	10.83
LG-50DT45F	554.18	558.82	0.84	97.87	91.38	6.63
LG-30DT0F	702.67	718.08	2.19	86.65	72.91	15.86
LG-30DT30F	640.83	646.91	0.95	87.90	76.19	13.32
LG-30DT45F	616.43	644.59	4.57	88.96	75.89	14.69

ratio (30) of various fiber orientations (±0°, ±30°, ±45°) is 13.99%, 15.05%, and 7.35% more than that of the columns containing the greater D/t ratio (50).

2) Strain analysis

The axial and hoop strain readings were evaluated by the strain gauges placed as illustrated in Fig. 8(b). The axial load vs the strain data (axial and hoop) were presented in Figs. 14(a)–14(c). The ultimate axial strain

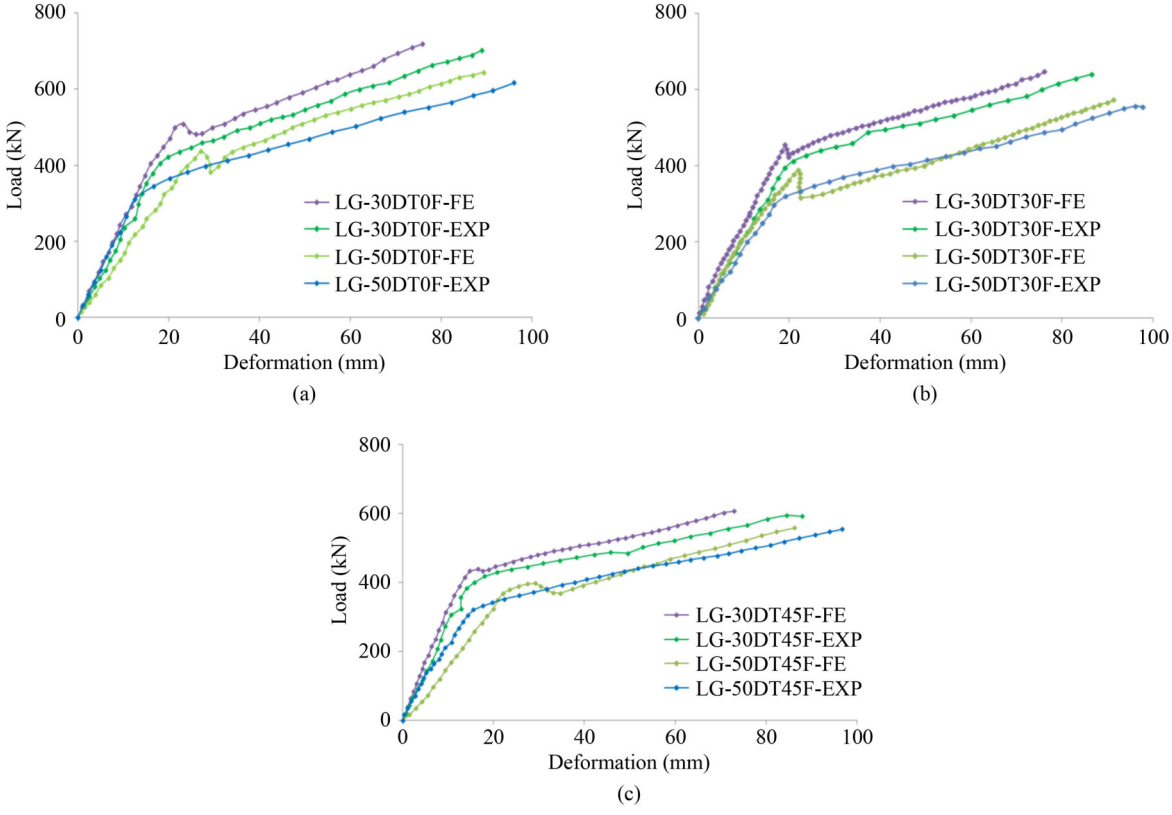

Fig. 13 Comparison of D/t ratio for load–deformation behavior for various fiber orientations: (a) ±0°; (b) ±30°; (c) ±45°.

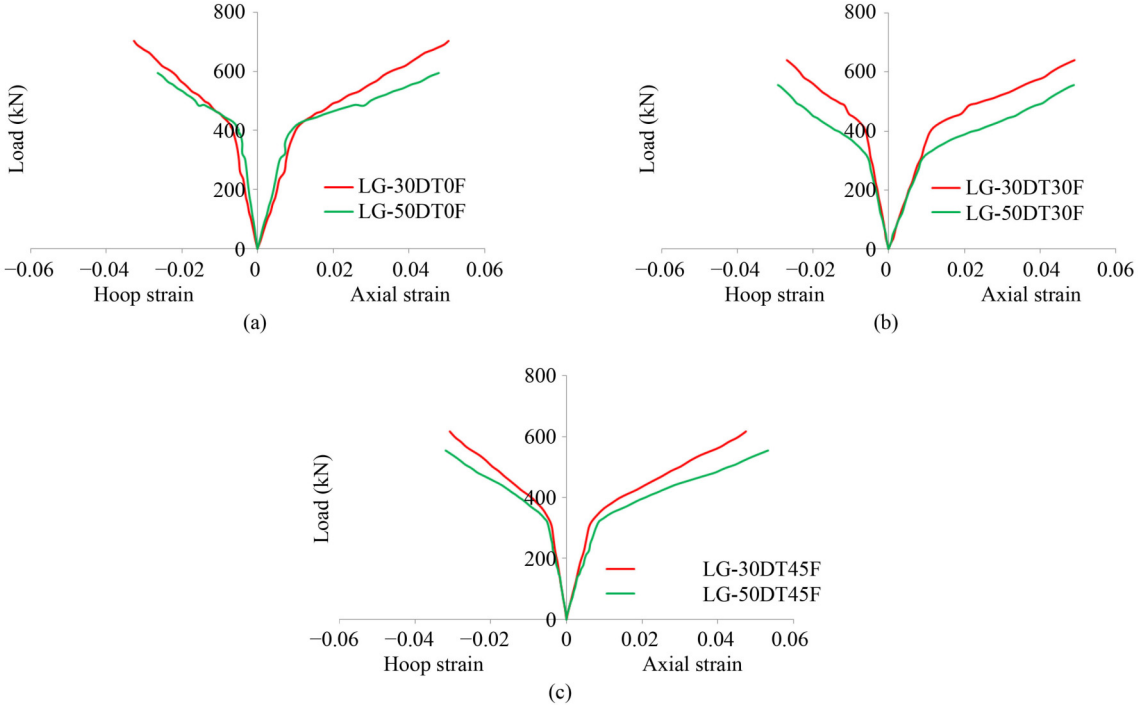

Fig. 14 Comparison of D/t ratio with respect to strain analysis for various fiber orientations: (a) ±0°; (b) ±30°; (c) ±45°.

value was in the range of 0.05 which is comparatively greater than the ultimate hoop strain of the columns which was around 0.03. The axial and hoop strain values were less than 0.01 till the load reaches 300 kN and it develops after reaching the yielding point from where the value increased gradually.

The strain data of the composite columns containing the lesser *D*/*t* ratio (30) were comparatively higher than the columns containing a greater *D*/*t* ratio (50) except for the columns with ±0° fiber orientations. It is mainly due to the better confinement ratio offered by the columns with a lesser *D*/*t* ratio (30). From Figs. 14(a)–14(c), it is witnessed that the axial strain value was greater than the hoop strain value of these LWSCGC-GFRP composite columns under axial compressive loading.

4.1.3.2 The impact of fiber orientation

1) Load-deformation behavior

The fiber orientations of ±0°, ±30°, and ±45° were compared among the two *D*/*t* ratios 30 and 50. However the fiber orientation is associated with the GFRP tube alone, It influences the property of the whole composite column. It can be evident from Figs. 15(a) and 15(b), that fiber orientation has a significant effect on the axial performance of these LWSCGC-GFRP composite columns. The performance of the columns containing ±0° fiber orientation is comparatively greater than the columns containing any other fiber orientations (±30° and ±45°). The columns exhibit a similar pattern in the first phase and the difference in the load is seen in the second phase of the load−deformation curve.

Among the column category of lesser *D*/*t* ratio (30), the column with fiber orientation of ±0° is 9.65 and 18.11% greater than the columns with fiber orientations of ±30° and ±45°. Comparing the fiber orientations in the column category of greater *D*/*t* ratio (50), the composite column containing the fiber orientation of ±0° is 10.67 and 11.23% greater than the columns with fiber orientations of ±30° and ±45°. From this study, it can be inferred that the columns with fiber orientation of ±0° hold good performance than any other orientations used in the study and it is mainly due to the complete confinement of fibers in the GFRP tube.

2) Strain analysis

The axial and hoop strain data were recorded and compared with the different fiber orientations. As inferred in the previous Subsection 4.1.3.1, the ultimate axial strain data was higher than the ultimate hoop strain data. From Figs. 16(a) and 16(b), it is found that the fiber

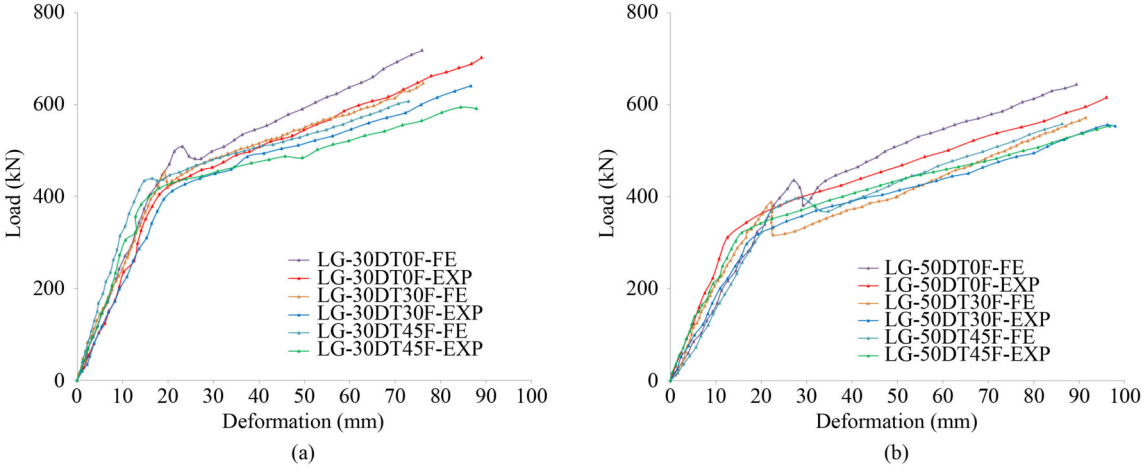

Fig. 15 The impact of fiber orientation with respect to load−deformation for different *D*/*t* ratio: (a) 30; (b) 50.

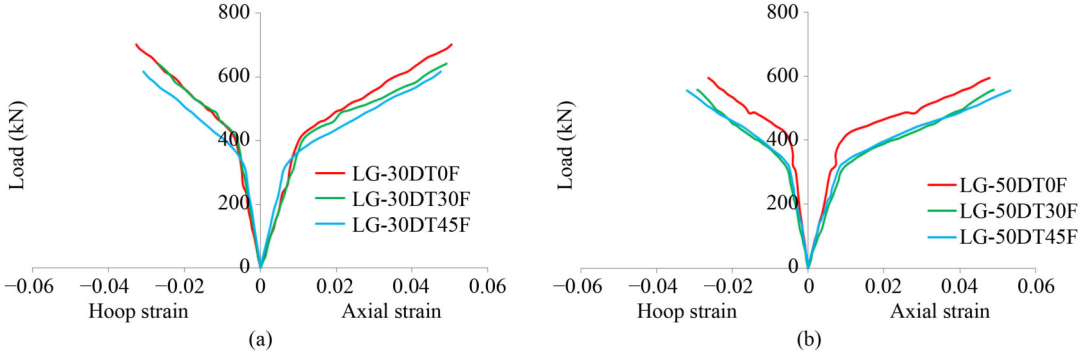

Fig. 16 The impact of fiber orientation with respect to strain analysis for various *D*/*t* ratios: (a) 30; (b) 50.

orientation has a considerable impact on the strain analysis. In the columns containing a lesser D/t ratio (30), the strain values of the column containing ±0° fiber orientation are greater than the other orientations (±30° and ±45°). In the columns containing the greater D/t ratio (50), the strain values of the column with ±45° are comparatively higher than the other orientations (±0° and ±30°).

5 Theoretical study

Few theoretical predictions were available for evaluating the approximate axial load of concrete in-filled FRP composite columns. The obtained experimental and numerical results were compared with those theoretical models.

5.1 Review of prediction models

5.1.1 ACI 440.2R-08 [48]

The ACI 440.2R-08 represents the axial load resistance (P_r) of the concrete in-filled FRP confined columns by the rational Eq. (1)

$$P_r = \varnothing P_n = 0.85\varnothing\left[0.85f'_{cc}\left(A_g - A_s\right) + f_y A_s\right], \quad (1)$$

where $\varnothing = 0.65$ for the tied columns, f'_{cc} is the compressive strength with confinement which is derived from the Lam and Teng model (2)

$$f'_{cc} = f'_c + \varphi_f 3.3 K_a f_{lFRP}, \quad (2)$$

where f'_c is the compressive strength without confinement, $\varphi_f = 0.95$ is another factor, K_a is the efficiency factor primarily based on the cross-section and $K_a = 1$ for the circular sections, f_{lFRP} can be given by Eq. (3)

$$f_{lFRP} = \frac{2E_{FRP} n t_{FRP} \varepsilon_{fe}}{D}, \quad (3)$$

where $\varepsilon_{fe} = K_\varepsilon \varepsilon_{fu}$ is the strain efficiency factor and $K_\varepsilon = 0.55$ is an additional strain efficiency factor given by Pessiki et al., A_g is the gross area, A_s and f_y are the total area and yield stress of steel.

5.1.2 CSA S806-02 [49]

The CSA S806-02 has given the equation for calculating the axial load (P_r) of RC members with lateral confinement. Equation (4) is as follows.

$$P_r = K_e\left[\propto_1 \varnothing_c f'_{cc}\left(A_g - A_s\right) + \varnothing_s f_y A_s\right], \quad (4)$$

where $K_e = 0.85$, $\propto_1 = 0.85 - 0.0015 f'_c \geqslant 0.39$, $\varnothing_c = 0.60$, $\varnothing_s = 0.85$, and f'_{cc} is given by Eq. (5)

$$f'_{cc} = 0.85 f'_c + k_1 k_s f_{lFRP}, \quad (5)$$

where k_1 is the additional factor given by $k_1 = 6.7(f_{lFRP})^{-0.17}$, $k_s = 1$ for the circular section and f_{lFRP} is given by (6)

$$f_{lFRP} = \frac{2t_{FRP}\varnothing_{FRP} f_{FRPu}}{D} \leqslant \frac{2t_{FRP} E_{FRP} 0.004}{D}, \quad (6)$$

where $\varnothing_{FRP} = 0.65$ is an additional resistance factor, and the code permits the hoop strain up to 0.004 times its elastic modulus E_{FRP}.

5.1.3 Mohamed et al. model [59]

After reviewing various codes, Mohamed et al. [59] proposed an Eq. (7) with various crucial factors for predicting the ultimate load for the concrete columns strengthened by FRP confinement with steel reinforcement.

$$P_r = 0.85\varnothing k_{cr}\left[k_{cc} f'_{cc}\left(A_g - A_s\right) + f_y A_s\right], \quad (7)$$

where $\varnothing$ is the additional reduction factor and can be taken as 0.75 as per ACI codal provisions [60], k_{cr} is the additional factor for the concrete cracking and yielding of steel, k_{cc} is a new factor which is the ratio of f'_{cc} and f'_c. In this model, f'_{cc} is given by the expression (8)

$$f'_{cc} = f'_c\left[0.7 + 2.7\left(\frac{f_{lFRP}}{f'_c}\right)^{0.7}\right]. \quad (8)$$

The experimental values were validated against these models and Mohamed et. al model performs better with an error percentage of 6.18% whereas the ACI 440.2R-08 and CSA for Building Code perform with an error percentage of 13.93% and 9.64% The experimental observations were tested with various prediction models and the difference in the error percentage was calculated and is presented in Table 6.

5.2 Proposed model

By validating the experimental results with these various prediction models, a new theoretical model is presented for determining the axial load of the confined reinforced concrete columns. These prediction models vary due to the changes in the factors employed with the equations. The model given by Mohamed et. al outperforms the outcomes obtained from the other models. However, the reduction factors play a predominant role in predicting those values. The additional reduction factor ($\varnothing$) has been taken as 0.75 as prescribed in the ACI. This reduction factor could not be the same in every case due to the various unexpected scenarios. The maximum reduction factor can be taken as 0.75. It could not be a fixed value and may vary for different cases. The additional reduction

Table 6 Comparison of experimental results with various models

Column	Load (Experimental)	Existing models			Proposed model	Percentage Error (Proposed vs Existing models)		
		ACI 440.2 R-08	CSA-S806-02	Mohamed et al.		ACI 440.2 R-08	CSA-S806-02	Mohamed et al.
LG-50DT0F	594.91	545.65	588.25	564.21	598.06	8.76	1.64	5.66
LG-50DT30F	557.00	523.74	545.99	523.23	564.63	7.24	3.30	7.33
LG-50DT45F	554.18	515.51	544.72	518.99	557.13	7.47	2.23	6.85
LG-30DT0F	702.67	689.48	679.48	682.44	703.39	1.98	3.40	2.98
LG-30DT30F	640.83	651.91	645.21	640.22	668.64	2.50	3.50	4.25
LG-30DT45F	616.43	649.95	644.95	626.31	633.89	2.53	1.74	1.20
Mean square error (Experimental VS Analytical)		0.86	0.90	0.94	0.97	N/A*	N/A*	N/A*

*Note: N/A: Not applicable.

factor can be taken as a floating value from 0.75 to 0.85 and it could have a better impact on every case.

Increasing the additional reduction factor from 0.75 to 0.85 has almost good accuracy with an error percentage of 3%–4%. In this proposed model, the axial load (P_r) for the confined concrete columns with steel reinforcement can be given by Eq. (9)

$$P_r = 0.85 \varnothing_a k_{cr} \left[k_{cc} f'_{cc} \left(A_g - A_s \right) + f_y A_s \right], \tag{9}$$

where $\varnothing_a = 0.75$–0.85.

The experimental data were validated with the proposed model presented in Table 6, and the percentage error obtained is comparatively less than the previous models with R^2 of 0.97.

6 Conclusions

This research examines the behavior of the novel concrete material (LWSCGC) in-filled GFRP tubular columns under axial compressive loading by experimental, numerical, and theoretical methods. This research comes up with the following conclusions.

1) The development of innovative concrete involves incorporating industrial and agricultural waste products, using alternative binders like GGBS and RHA instead of the traditional OPC. This reduces the carbon footprint and promotes environmentally friendly and sustainable construction practices.

2) The concrete mix is lightweight and self-compacting, making it an efficient material for various structural elements. It provides a long-lasting and durable solution that will stand the test of time. By using this type of concrete, carbon footprint can be reduced and contribute to a sustainable future.

3) These LWSCGC-GFRP composite columns failed under axial compression loading and the common failure modes observed were the rupturing of the GFRP tube and buckling of the column in both experimental and FE analyses. Bonding failure of the concrete and GFRP tube, as well as the concrete and reinforcement steel, were noticed only in the experiments.

4) The load−deformation pattern of these LWSCGC-GFRP composite columns was the gradual increase in the load with smaller deformation till yielding and the gradual increase in the load continues with greater deformation until failure.

5) Using FRP tubes with a lower D/t ratio has been found to increase the ability of CFFT columns to withstand higher lateral loads with less lateral displacement. Additionally, studies have shown that CFFT columns with fibers oriented in the hoop direction (0°) possess even greater lateral load-carrying capacity while maintaining minimal lateral displacement. This information can be valuable for engineers and designers looking to optimize the performance of CFFT columns.

6) Comparing the LWSCGC-GFRP composite columns, the axial performance of columns containing a lesser D/t ratio (30) (LG-30DT0F, LG-30DT30F, and LG-30DT45F) is 13.99%, 15.05%, and 7.35% higher than those of the columns containing greater D/t ratio (50) (LG-50DT0F, LG-50DT30F, and LG-50DT45F). This indicates that increasing the D/t ratio decreases the overall axial performance of the columns.

7) In the columns category of lesser D/t ratio (30), the axial performance of the column containing the fiber orientation of ±0° (LG-30DT0F) is 9.65% and 18.11% greater than the columns with fiber orientations of ±30° and ±45° in D/t ratio of 30 (LG-30DT30F, and LG-30DT45F). Similarly, in the category of greater D/t ratio (50), the column (LG-50DT0F) is 10.67% and 11.23% greater than their corresponding columns (LG-50DT30F and LG-50DT45F). It can be inferred that the LWSCGC-GFRP composite columns containing the ±0° fiber orientation have greater efficiency related to axial compressive performance.

8) The designed FE model is validated against the experiment and the results were quite comparable with very low errors ranging from 0.84% to 4.57%. This numerical model can be utilized for predicting the Lightweight concrete in-filled FRP composite columns.

9) The experimental results were compared and validated against various theoretical prediction models and have an error percentage ranging from 7% to 14%. A

new theoretical prediction model is proposed and validated with the experimental values and the results were quite comparable with an error percentage of 3.3%.

However, the axial compressive performance of this innovative lightweight concrete filled FRP composite columns were investigated in this study. The seismic performance of these lightweight concrete filled FRP composite columns can be taken as the future scope of this study for determining the capacity of the columns when exposed to the seismic activities.

Acknowledgements The authors acknowledged the support by All India Council for Technical Education (AICTE) under Research Promotion Scheme; File No. 8232/RIFD/RPS (POLICY-1)/2018-19.

Competing interests The authors declare that they have no competing interests.

References

1. Hardjito D, Rangan B V. Development and Properties of Low-Calcium Fly Ash-Based Geopolymer Concrete. Perth: Curtin University of Technology, 2005
2. Temuujin J, van Riessen A, MacKenzie K J D. Preparation and characterisation of fly ash based geopolymer mortars. Construction and Building Materials, 2010, 24(10): 1906–1910
3. Davidovits J. Geopolymer cement to minimize carbon-dioxde greenhouse-warming. Ceramic Transactions, 1993, 37: 165–182
4. Kurtoglu A E, Alzeebaree R, Aljumaili O, Nis A, Gulsan M E, Humur G, Cevik A. Mechanical and durability properties of fly ash and slag based geopolymer concrete. Advances in Concrete Construction, 2018, 6(4): 345
5. Ryu G S, Lee Y B, Koh K T, Chung Y S. The mechanical properties of fly ash-based geopolymer concrete with alkaline activators. Construction and Building Materials, 2013, 47: 409–418
6. Li X, Ma X, Zhang S, Zheng E. Mechanical properties and microstructure of class C fly ash-based geopolymer paste and mortar. Materials, 2013, 6(4): 1485–1495
7. Davidovits J, Orlinski J. Geopolymer International Conference Proceedings. Geopolymer Institute, 1999
8. Nazari A, Sanjayan J G. Modelling of compressive strength of geopolymer paste, mortar and concrete by optimized support vector machine. Ceramics International, 2015, 41(9): 12164–12177
9. Rangan B V, Hardjito D, Wallah S E, Sumajouw D M. Studies on fly ash-based geopolymer concrete. In: Proceedings of the World Congress Geopolymer. France: Saint Quentin, 2005, 28: 133–137
10. Chindaprasirt P, Chareerat T, Sirivivatnanon V. Workability and strength of coarse high calcium fly ash geopolymer. Cement and Concrete Composites, 2007, 29(3): 224–229
11. Guo X, Shi H, Dick W A. Compressive strength and microstructural characteristics of class C fly ash geopolymer. Cement and Concrete Composites, 2010, 32(2): 142–147
12. Sayyad A S, Patankar S V. Effect of steel fibres and low calcium fly ash on mechanical and elastic properties of geopolymer concrete composites. Indian Journal of Materials Science, 2013, 2013(1): 357563
13. Nath P, Sarker P K, Rangan V B. Early age properties of low-calcium fly ash geopolymer concrete suitable for ambient curing. Procedia Engineering, 2015, 125: 601–607
14. Memon S A, Shaikh M A, Akbar H. Utilization of rice husk ash as viscosity modifying agent in self compacting concrete. Construction and Building Materials, 2011, 25(2): 1044–1048
15. Saha S, Rajasekaran C. Enhancement of the properties of fly ash based geopolymer paste by incorporating ground granulated blast furnace slag. Construction and Building Materials, 2017, 146: 615–620
16. Srishaila J M, Ahamed P P, Vishwanath K N, Prakash P. Experimental study on workability and strength characteristics of fly ash and GGBS based self-compacting geo polymer concrete. International Engineering Journal for Research and Development, 2014, 10(6): 68–77
17. Venkatesan R P, Pazhani K C. Strength and durability properties of geopolymer concrete made with ground granulated blast furnace slag and black rice husk ash. KSCE Journal of Civil Engineering, 2016, 20(6): 2384–2391
18. Khayat K H. Workability, testing, and performance of self-consolidating concrete. Materials Journal, 1999, 96(3): 346–353
19. Rossignolo J A, Agnesini M V, Morais J A. Properties of high-performance LWAC for precast structures with Brazilian lightweight aggregates. Cement and Concrete Composites, 2003, 25(1): 77–82
20. Bartolini R, Filippozzi S, Princi E, Schenone C, Vicini S. Acoustic and mechanical properties of expanded clay granulates consolidated by epoxy resin. Applied Clay Science, 2010, 48(3): 460–465
21. Shebannavar H, Maneeth P D, Brijbhushan S. Comparative study of LECA as a complete replacement of coarse aggregate by ACI method with equivalent likeness of strength of is method. International Research Journal of Engineering and Technology, 2015, 2(8): 589–594
22. Bodnárová L, Hela R, Hubertová M, Nováková I. Behaviour of lightweight expanded clay aggregate concrete exposed to high temperatures. International Journal of Civil and Environmental Engineering, 2014, 8(12): 1210–1213
23. Nematollahi B, Ranade R, Sanjayan J, Ramakrishnan S. Thermal and mechanical properties of sustainable lightweight strain hardening geopolymer composites. Archives of Civil and Mechanical Engineering, 2017, 17(1): 55–64
24. Ilki A, Peker O, Karamuk E, Demir C, Kumbasar N. FRP retrofit of low and medium strength circular and rectangular reinforced concrete columns. Journal of Materials in Civil Engineering, 2008, 20(2): 169–188
25. Jamatia R, Hussain T, Deb A, Bhattacharyya S K. Effect of imperfections in the bond on the strength of FRP wrapped cylindrical concrete columns. Composites. Part B, Engineering, 2013, 53: 297–307
26. Campione G, La Mendola L, Monaco A, Valenza A, Fiore V. Behavior in compression of concrete cylinders externally wrapped with basalt fibers. Composites. Part B, Engineering, 2015, 69: 576–586

27. Yazdani N, Goucher E. Increasing durability of lightweight concrete through FRP wrap. Composites. Part B, Engineering, 2015, 82: 166–172
28. Saljoughian A, Mostofinejad D. Axial-flexural interaction in square RC columns confined by intermittent CFRP wraps. Composites. Part B, Engineering, 2016, 89: 85–95
29. Ozbakkaloglu T, Louk Fanggi B A. FRP–HSC–steel composite columns: Behavior under monotonic and cyclic axial compression. Materials and Structures, 2015, 48(4): 1075–1093
30. Zhang B, Yu T, Teng J G. Behavior of concrete-filled FRP tubes under cyclic axial compression. Journal of Composites for Construction, 2015, 19(3): 04014060
31. Boumarafi A, Abouzied A, Masmoudi R. Harsh environments effects on the axial behaviour of circular concrete-filled fibre reinforced-polymer (FRP) tubes. Composites. Part B, Engineering, 2015, 83: 81–87
32. Xie T, Ozbakkaloglu T. Behavior of steel fiber-reinforced high-strength concrete-filled FRP tube columns under axial compression. Engineering Structures, 2015, 90: 158–171
33. Lokuge W, Karunasena W. Ductility enhancement of geopolymer concrete columns using fibre-reinforced polymer confinement. Journal of Composite Materials, 2016, 50(14): 1887–1896
34. Ozbakkaloglu T, Xie T. Geopolymer concrete-filled FRP tubes: Behavior of circular and square columns under axial compression. Composites. Part B, Engineering, 2016, 96: 215–230
35. Padanattil A, Lakshmanan M, Jayanarayanan K, Mini K M. Strengthening of plain concrete cylinders with natural FRP composite systems. Civil Engineering, 2019, 43(3): 381–389
36. Zhou Y, Liu X, Xing F, Li D, Wang Y, Sui L. Behavior and modeling of FRP-concrete-steel double-skin tubular columns made of full lightweight aggregate concrete. Construction and Building Materials, 2017, 139: 52–63
37. Kurtoğlu A E, Hussein A K, Gülşan M E, Çevik A. Flexural behavior of HDPE tubular beams filled with self-compacting geopolymer concrete. Thin-walled Structures, 2021, 167: 108096
38. Bhatt P P, Kodur V K, Shakya A M, Alkhrdaji T. Performance of insulated FRP-strengthened concrete flexural members under fire conditions. Frontiers of Structural and Civil Engineering, 2021, 15(1): 177–193
39. Abbood I S, aldeen Odaa S, Hasan K F, Jasim M A. Properties evaluation of fiber reinforced polymers and their constituent materials used in structures—A review. Materials Today: Proceedings, 2021, 43: 1003–1008
40. Roy M, Hollmann C, Wille K. Influence of fiber volume fraction and fiber orientation on the uniaxial tensile behavior of rebar-reinforced ultra-high performance concrete. Fibers, 2019, 7(7): 67
41. Vincent T, Ozbakkaloglu T. Influence of fiber type on behavior of high-strength concrete-filled FRP tubes under concentric compression. Applied Mechanics and Materials, 2013, 438: 240–245
42. Totonchi A, Ansaripour A, Shivaei S. Effect of different arrangements of CFRP wraps on the axial stress–strain behaviour of confined concrete cylinders: Experimental study and numerical modelling. Civil Engineering, 2020, 44(4): 1087–1100
43. Mirmiran A, Shahawy M. Behavior of concrete columns confined by fiber composites. Journal of Structural Engineering, 1997, 123(5): 583–590
44. Karbhari V M, Gao Y. Composite jacketed concrete under uniaxial compression—Verification of simple design equations. Journal of Materials in Civil Engineering, 1997, 9(4): 185–193
45. La Tegola A, Manni O. Experimental investigation on concrete confined by fiber reinforced polymer and comparison with theoretical model. Special Publication, 1999, 188: 243–254
46. Fanggi B A L, Ozbakkaloglu T. Compressive behavior of aramid FRP–HSC–steel double-skin tubular columns. Construction and Building Materials, 2013, 48: 554–565
47. Raza A, Ali B, Rehman A. Structural performance of steel-tube concrete columns confined with CFRPs: Numerical and theoretical study. Civil Engineering, 2021, 45(3): 1575–1592
48. ACI 440.2 R-08. Guide for the Design and Construction of Externally Bonded FRP Systems for Strengthening Concrete Structures. Farmington Hills, MI: ACI, 2008
49. S806-02. Design and Construction of Building Components with Fibre-Reinforced Polymers. Mississauga: Canadial Standards Association, 2002
50. Tang H, Liu R, Zhao X, Guo R, Jia Y. Axial compression behavior of CFRP-confined rectangular concrete-filled stainless steel tube stub column. Frontiers of Structural and Civil Engineering, 2021, 15(5): 1144–1159
51. BIBM. The European Guidelines for Self-Compacting Concrete. 2005, 22: 563
52. ASTM. Standard Test Method for Tensile Properties of Polymer Matrix Composites Materials. ASTM D3039M-08, West Conshohocken, PA: ASTM, 2008
53. ASTM. Standard Test Method for Apparent Hoop Tensile Strength of Plastic or Reinforced Plastic Pipe. ASTM D2290-12, West Conshohocken, PA: ASTM, 2006
54. ASTM. Standard Test Methods and Definitions for Mechanical Testing of Steel Products. ASTM 370-20, West Conshohocken, PA: ASTM, 2014
55. Ren Z, Zeng X, Shen Y, Huang H. Axial compression test and bearing capacity analysis of biaxial prestressed angle steel plate fully wrapped reinforced concrete short column. Advances in Civil Engineering, 2022, 2022: 2022
56. Ji J, Li J, Jiang L, Ren H, Wang Q, Wang X, He L, Zhang Z. Mechanical behavior of special-shaped reinforced concrete composite columns encased with GFRP core columns. Buildings, 2022, 12(11): 1895
57. Ji J, Wang W, Jiang L, Ren H, Wang Q, Xuan W, Liu Y. Bearing capacity of UHPC-filled high-strength elliptical steel tube composite columns with encased high-strength H-shape steel subjected to eccentrical load. Buildings, 2022, 12(8): 1272
58. Shao Y, Aval S, Mirmiran A. Fiber-element model for cyclic analysis of concrete-filled fiber reinforced polymer tubes. Journal of Structural Engineering, 2005, 131(2): 292–303
59. Mohamed H M, Masmoudi R. Axial load capacity of concrete-filled FRP tube columns: Experimental versus theoretical predictions. Journal of Composites for Construction, 2010, 14(2): 231–243
60. ACI. Building Code Requirements for Structural Concrete and Commentary. ACI 318-08, Farmington Hills, MI: ACI, 2008